

Nonlocal Power Deposition in Inductively Coupled Plasmas

John D. Evans* and Francis F. Chen†

Electrical Engineering Department, University of California, Los Angeles, Los Angeles, California 90095-1594
(Received 26 February 2001)

Radiofrequency (rf) plasmas exhibit field penetration well beyond the classical skin depth. Two physical explanations are proposed. First, by tracing orbits of electrons through many rf cycles in a cylindrical system, it is shown that numerous ionizing electrons can reach the interior. Second, current-carrying electrons can form a long-lived torus that drifts toward the axis, causing frequently observed interference phenomena. The pressure dependence of this effect does not agree with collisionless theories of anomalous skin effect, but is consistent with the proposed mechanism.

DOI: 10.1103/PhysRevLett.86.5502

PACS numbers: 52.77.-j, 52.20.Dq, 52.50.-b, 52.80.Pi

The anomalous skin effect [1] (ASE) has intrigued plasma researchers since the 1960s, when Demirkhanov *et al.* [2] and others [3] reported nonmonotonic decay of rf fields in an overdense plasma. This problem has resurfaced with the use of inductively coupled plasmas (ICPs) in the fabrication of integrated circuits and micro-electro-mechanical systems. Although rf plasma sources are indispensable for the computer industry, the physics of rf plasma production is not fully understood. In particular, nonlocal phenomena, in which currents do not obey the local form of Ohm's law, have been observed [4]. We address two such effects: (i) penetration of rf energy well beyond the classical skin layer, and (ii) nonmonotonic behavior of the rf field with radius. Effect (i) was observed in the device shown in Fig. 1, consisting of a four-turn loop antenna encircling a 30-cm-diam, 10-cm-long, 1.3-cm-thick glass bell jar that sits on top of a somewhat larger chamber. Time-averaged profiles of density $n(r)$, electron temperature $T_e(r)$, and space potential $V_s(r)$ were obtained with an rf-compensated Langmuir probe; and axial rf magnetic field $B_z(r)$ profiles were measured with a 5-mm-diam, three-turn magnetic probe in the plane of the antenna. Figure 2 shows that, under typical operating conditions, $n(r)$ is flat or peaked near the axis, even though the rf power is concentrated in a ≈ 3 -cm thick skin layer near the boundary $r = a$, and axial diffusive losses should lead to a hollow profile. $T_e(r)$ has a small peak in the skin layer, as expected, and both T_e and V_s are nearly constant in the interior region. Even flatter $n(r)$ were obtained in a commercial ICP (PlasmaTherm, Inc.) via diffusion into a lower chamber. This anomaly has been reported elsewhere [5].

Attempts at explaining nonlocal behavior have been based on two concepts: nonlocal conductivity [4,6,7] due to thermal motions (ASE), and the nonlinear ponderomotive force. A kinetic explanation was proposed by Weibel [8] in 1967. In plane geometry, a small class of electrons making a glancing angle with the wall remain in the skin layer long enough to acquire large energies from the E -field induced by the antenna. These fast electrons then wander into the interior region via thermal motions. This

theory was extended to cylindrical geometry by Sayasov [9] and has been espoused by many researchers [4,10–17]. The extensive, ongoing work by Godyak, Piejak, and others [4,11–15] is done with a spiral “stove-top” antenna with which the $n(r)$ anomaly is not apparent, since the antenna is radially distributed; indeed, no $n(r)$ profiles were shown. The second proposed mechanism is based on the Lorentz force \mathbf{F}_L due to the rf magnetic field \mathbf{B} , which exerts an inward force on the current-carrying electrons and also generates a second-harmonic rf field. The latter effect has been studied by Piejak, Godyak *et al.* [18–21] and others [22–25].

By tracing individual electron orbits in the rf field of a cylindrical system, we find that ASE is greatly enhanced over that predictable from T_e alone. Wall curvature causes electrons to impinge upon the wall sheath at steeper angles, reflecting them into the interior regions. This effect is further enhanced by \mathbf{F}_L . Figure 3(a) shows the path of an electron starting with $|\mathbf{v}| = 0$ at a radius inside the skin layer in

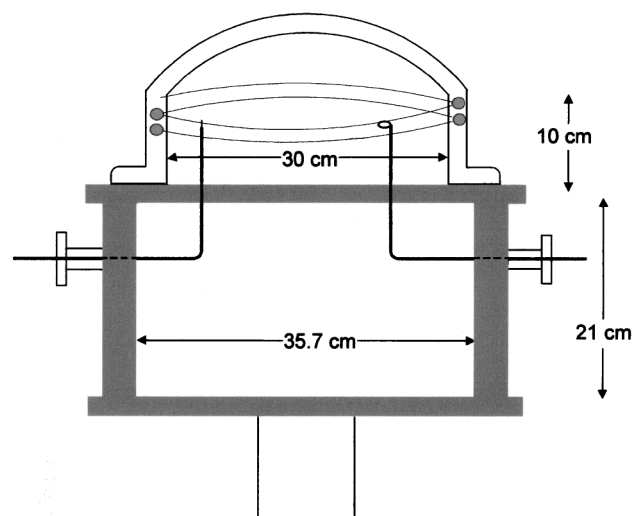


FIG. 1. Device schematic, showing radially scannable B-dot (right) and Langmuir (left) probes located in the plane of the multiturn loop antenna.

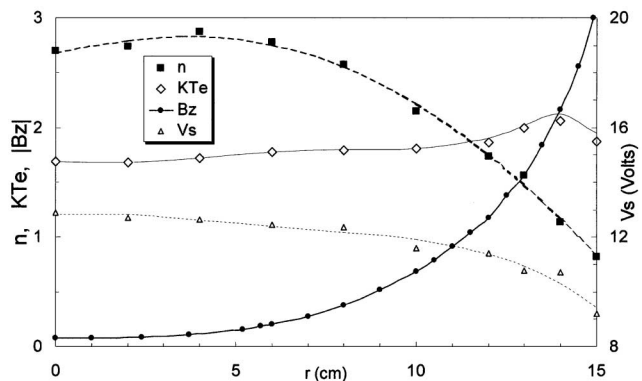


FIG. 2. Profiles of n (10^{11} cm^{-3}), KT_e (eV), V_s (V), and B_z (arbitrary units) in an ICP discharge in 10 mTorr of argon, with $P_{\text{rf}} = 300 \text{ W}$ at 2 MHz.

an rf field given by $E_\theta = E_0[I_1(k_s r)/I_1(k_s a)] \sin \omega t$, $B_z = (k_s/\omega)E_0[I_0(k_s r)/I_1(k_s a)] \cos \omega t$, where I_0 , I_1 are Bessel functions, and $k_s \equiv 1/d_s$. In these 2D calculations, the skin depth d_s , frequency ω , radius a , and field strength E_0 are prescribed using experimental values. Initial particle position (r, θ) and velocity (v_r, v_θ) can be varied, as well as the initial phase $\phi = \omega t_0$. Specular reflection off the Coulomb barrier at the sheath edge is assumed, and sheath thickness is neglected compared with d_s . Electrons reflect at steep angles from the wall after only a few rf periods (τ_{rf}) and rapidly reach the interior regions. The Lorentz force \mathbf{F}_L enhances this effect by imparting radial momentum. Figure 3(b) together with 3(a), shows that the electron energy exceeds the ionization energy only near the wall without \mathbf{F}_L but is large even in the interior with \mathbf{F}_L . Individual trajectories vary greatly with E_0 and the initial values \mathbf{r}_0 , \mathbf{v}_0 , and ϕ_0 , but examination of many cases reveals several trends: (i) Almost all orbits reach the interior after a few τ_{rf} regardless of \mathbf{F}_L , but their energies in the interior are higher when \mathbf{F}_L is included; (ii) the effect of \mathbf{F}_L is larger at lower ω and when the transit time across a diameter is on the order of τ_{rf} , (iii) electrons born in the interior remain in this weak-field region for many cycles, enhancing $n(r)$ there with their long residence time, but eventually reach the skin layer and get accelerated; (d) the initial electron thermal velocity makes little difference, since they gain much more energy from the rf field.

A more realistic model includes elastic and inelastic collisions, electron loss to the wall, and replenishment via ionization. The electron equation of motion is

$$d\mathbf{v}/dt = (-e/m)(\mathbf{E} + \mathbf{v} \times \mathbf{B}) - \nu_c \mathbf{v}, \quad (1)$$

where \mathbf{E} , \mathbf{B} , and collision frequency ν_c are evaluated at the local values of \mathbf{r} and \mathbf{v} . The collision probability for a given neutral pressure p is recalculated at each time step. If the electron collides elastically, it proceeds with the same velocity in a random direction. Inelastic collisions comprise $<0.1\%$ of all collisions and are thus negligible in the orbit calculations. When an electron reaches the sheath,

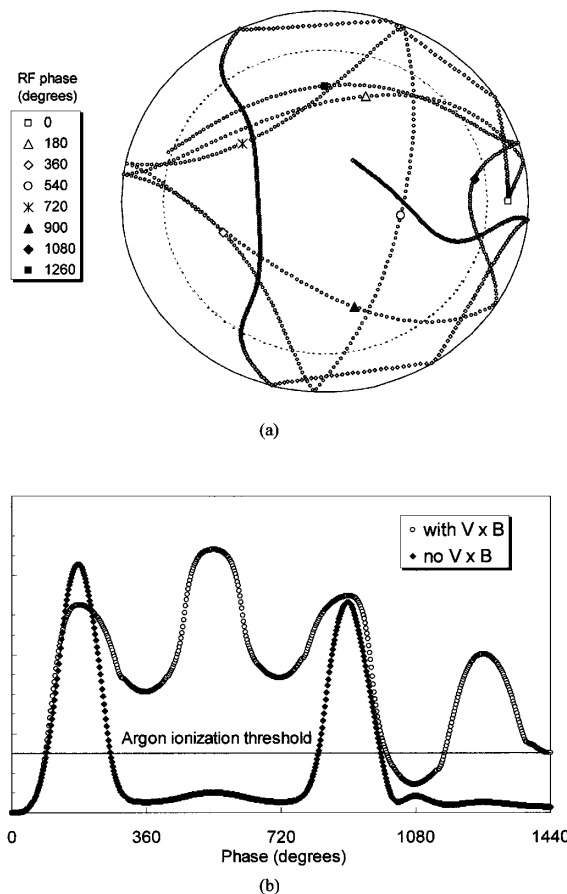


FIG. 3. (a) Path of an electron starting at rest (\square) during the first four cycles of a 6.78 MHz rf field $E_\theta \sin \omega t$, with (marked path) and without (unmarked path) inclusion of the $\mathbf{v} \times \mathbf{B}$ force \mathbf{F}_L . The triangles (Δ) mark the positions where E_θ changes sign. The points are 1 ns apart. The outer circle is the sheath boundary at $r = a$, and the inner circle is smaller by a skin depth of 3.1 cm. $E_\theta(a) = -8 \text{ V/cm}$; $B_z(a) = -7 \text{ G}$. (b) Energy of the electrons following the orbits in (a). The upper curve includes \mathbf{F}_{NL} ; the lower does not. The line shows the ionization threshold in argon.

it is reflected unless its perpendicular energy is larger than a prescribed sheath voltage V_{sh} . In the latter case, it is lost and replaced by an electron with random (\mathbf{r}, \mathbf{v}) , weighted according to a prescribed T_e . Experimentally determined V_{sh} and T_e are used. A typical orbit over $67\tau_{\text{rf}}$ is shown in Fig. 4; discontinuities due to collisions and wall losses can be seen. By following an electron and its reincarnations over many τ_{rf} , one can construct an ensemble average of the electron energy distribution function (EEDF) and density at each radius. Figure 5 shows histograms of n and EEDF in four radial sectors of equal area, computed for the conditions of Fig. 2 and comprising 320 000 (\mathbf{r}, \mathbf{v}) pairs. It is seen that there are more low-energy electrons in the weak-field regions, as expected, but that a population of fast electrons capable of ionization exists in all regions, far in excess of those in a Maxwellian distribution. Electron accumulation near $r = 0$ reduces V_s there, thus increasing $n_i(r)$ locally via reduced ambipolar loss. This mechanism can lead to the centrally peaked $n(r)$ of Fig. 2.

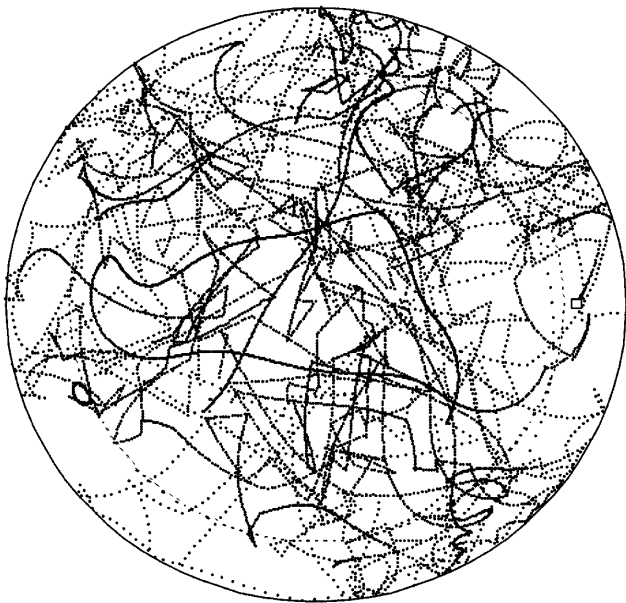


FIG. 4. A typical electron trajectory including collisions, losses through the sheath, and replenishment by ionization. Conditions: $f = 6.78$ MHz, $d_s = 3.1$ cm, $a = 15$ cm, $E_\theta = -8$ V/cm, $V_{sh} = 20$ V, $p = 10$ mTorr, $T_e = 3$ eV.

Effect (ii) is illustrated by Fig. 6, which shows that $|B_z|$ decays radially similar to a normal evanescent wave until it reaches $\approx 1\%$ of its maximum value. At $r \sim a/3$, local minima (nodes) appear, as well as a weak maximum on axis. The phase jumps by 180° across each node [26]. Similar profiles have been observed by a number of authors [2,10,11,13] who have attributed this effect to collisionless ASE. However, Fig. 6 shows that this “standing wave” effect is more pronounced at higher p (collisionality), in apparent contradiction to ASE theory. We propose an alternative physical explanation as follows. Since \mathbf{F}_L preferentially pushes the current-carrying electrons inward, these form a ring of current, which we call a current-carrying structure (CCS), detached from the background electrons. The B -field pattern of the CCS (Fig. 7) resembles a diffuse

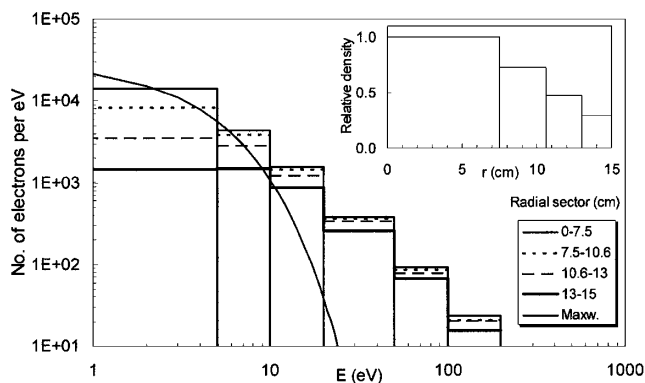


FIG. 5. Monte Carlo calculation of electron energy distribution in four radial regions of equal area. The inset shows the density profile. Conditions: $f = 2.0$ MHz, $d_s = 3.1$ cm, $a = 15$ cm, $E_\theta = -5$ V/cm, $V_{sh} = 20$ V, $p = 10$ mTorr, $T_e = 3$ eV. The curved line is a 3-eV Maxwellian distribution (log-log scale).

toroidal theta pinch. A CCS has an L/R decay time $\tau_{L/R}$ comparable to τ_{if} . Even at high p , the current is sustained because, if it should decay faster than $\tau_{L/R}$, the collapsing B -field of the CCS induces an azimuthal E -field to slow the decay. Formation of a CCS occurs in the skin layer during a maximum of E ($\phi \sim 0$) and comprises about half of the electron population. Note that the CCS is not composed solely of the fast ionizing electrons found in the orbit calculations above. As the CCS decays in the changing rf field, it is pushed inwards, maintaining an equilibrium position where the magnetic pressures inside and outside the ring are balanced. Radial motion of the CCS stagnates and reverses at $r/a \approx \frac{1}{3}$. As ϕ approaches 90° , the outside pressure drops, and the CCS begins to drift outwards. Near $\phi = 180^\circ$, a new CCS of opposite polarity is formed and pushed inwards until it meets the CCS from the previous half-cycle, which is now much weaker. The new CCS displaces the diminished one, and this process repeats every half-cycle. Since the CCS decays on its own time scale, it is out of phase with the normal skin current, giving rise to harmonics which are observed [18].

As a numerical example, consider a CCS with major radius R and minor radii b and c , where $c > b$ due to unfettered expansion in the z direction. For definiteness, assume a current distribution of the bi-Gaussian form,

$$j = j_0 \exp[-(r - R)^2/b^2] \exp(-z^2/c^2). \quad (2)$$

Assume initially $R_i = 12$, $b_i = 3$, and $c_i = 6$ cm. The self-inductance of this current distribution is computed to be $0.19 \mu\text{H}$ and is approximately doubled to $0.37 \mu\text{H}$ by the mutual inductance with the background plasma. For a CCS density $4 \times 10^{10} \text{ cm}^{-3}$ and a collision rate corresponding to 3-eV electrons in 10 mTorr of Ar, the computed resistance is $\approx 3.5 \Omega$, yielding $\tau_{L/R} \approx 0.1 \mu\text{s}$, comparable to the quarter-cycle time $\tau_{1/4}$ of $0.125 \mu\text{s}$. In its final position, we take $R_f = 5$, $b_f = 2.25$, and $c_f = 4.5$ cm, yielding $0.064 \mu\text{H}$ and 2.6Ω , for $\tau_{L/R} = 0.025 \mu\text{s}$. Thus, the CCS decays more rapidly as it moves

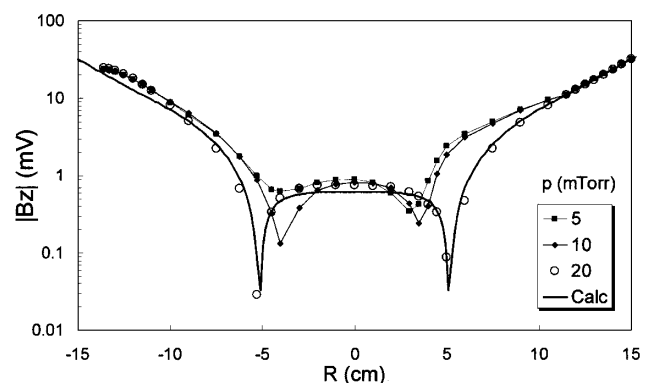


FIG. 6. Normalized semilog plot of $|B_z|(r)$ in the plane of the antenna at various pressures. The linear region corresponds to a skin depth of 3 cm. The 5- and 10-mTorr data are connected by lines, but the curve for the 20-mTorr data is a theoretical fit (see text). Conditions: 400 W at 2 MHz, 5–20 mTorr of Ar.

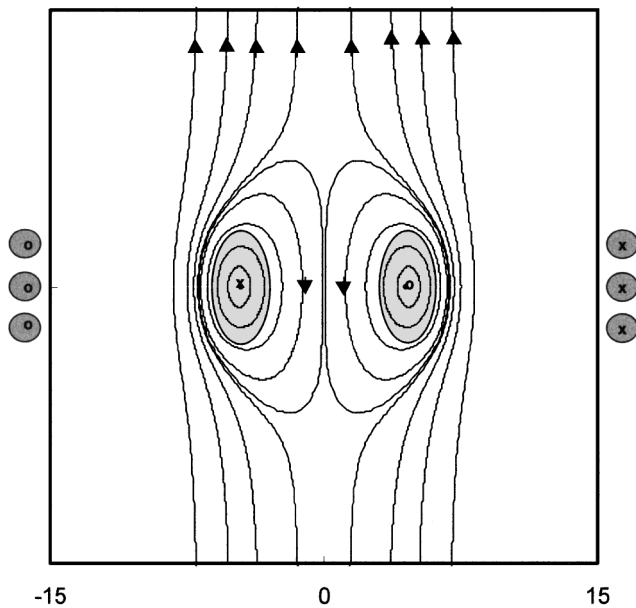


FIG. 7. Magnetic field lines around an elliptical, bi-Gaussian CCS with $R = 4.5$, $b = 1.5$, and $c = 3$ cm, imbedded in the time-averaged skin field of an $n = 8 \times 10^{10} \text{ cm}^{-3}$ plasma with $p = 10$ mTorr, $KT_e = 3$ eV, and $f = 2$ MHz. The box is 15×15 cm, and the curvature of the skin field is neglected. For clarity, the CCS current has been given a value higher than what it would be in practice.

inward and e -folds several times during an rf cycle. In Fig. 6, the 20-m Torr data are fitted with a CCS with $R = 7.5$, $b = 3$, and $c = 6$ cm, imbedded in a classical skin field with $n = 3 \times 10^{11} \text{ cm}^{-3}$, $p = 20$ mTorr, $KT_e = 3$ eV, and $f = 2$ MHz. Since $v_c/\omega \approx 5.4$ in this case, the field differs significantly from that in a collisionless, plane plasma [27]. Here, the CCS current was taken to be about four e -foldings below its initial current.

It is clear that the ratio $\rho \equiv \tau_{L/R}/\tau_{1/4}$ determines the magnitude of the standing wave effect. If ρ is too large, the CCS moves back and forth in each cycle, smearing out the null in the time-averaged $|B_z|$. If ρ is too small, the CCS decays away before reaching a radius where the background field is comparable to its field. Thus, effect (ii) occurs only in an optimal range of p and f , as is observed [10].

In conclusion, skin depth anomalies in ICPs can possibly be explained by two new mechanisms proposed here: the reflection of electrons off curved sheaths, and the generation of a detached current ring. The first mechanism suggests that antenna elements near the axis are not necessary for producing uniform plasmas. These effects are, of course, related and have been treated separately only to simplify the discussion. A large numerical simulation would probably yield an exact EEDF showing both features. Experiments can be performed to test these ideas, and the required computations may already exist, requiring only further diagnostics.

This work was supported by Applied Materials, Inc., and the Semiconductor Research Corporation. We thank PlasmaTherm, Inc. (now Unaxis) and Hiden Analytical, Ltd. for equipment loans, as well as Professor D. Arnush and Professor G. Tynan for insightful discussions.

*Electronic address: jdevans@ucla.edu

†Electronic address: ffchen@ee.ucla.edu

- [1] V. I. Kolobov and D. J. Economou, *Plasma Sources Sci. Technol.* **6**, R1 (1997), and references therein.
- [2] R. A. Demirkhanov, I. Ya. Kadysh, and Yu. S. Khodyrev, *Sov. Phys. JETP* **19**, 791 (1964).
- [3] M. J. Kofoed and J. M. Dawson, *Phys. Rev. Lett.* **17**, 1086 (1966).
- [4] V. I. Kolobov and V. A. Godyak, *IEEE Trans. Plasma Sci.* **23**, 503 (1995).
- [5] M. Tuszewski, *Phys. Rev. Lett.* **77**, 1286 (1996).
- [6] I. B. Bernstein and T. Holstein, *Phys. Rev.* **94**, 1475 (1954).
- [7] L. D. Tsengin, *Sov. Phys. JETP* **39**, 805 (1974).
- [8] E. S. Weibel, *Phys. Fluids* **10**, 741 (1967).
- [9] Yu. S. Sayasov, *Helv. Phys. Acta* **52**, 288 (1979).
- [10] B. Joye and H. Schneider, *Helv. Phys. Acta* **51**, 804 (1978).
- [11] V. A. Godyak and V. I. Kolobov, *Phys. Rev. Lett.* **79**, 4589 (1997).
- [12] V. A. Godyak and R. B. Piejak, *J. Appl. Phys.* **82**, 5944 (1997).
- [13] R. Piejak, V. A. Godyak, and B. Alexandrovich, *J. Appl. Phys.* **81**, 3416 (1997).
- [14] V. A. Godyak and V. I. Kolobov, *Phys. Rev. Lett.* **81**, 369 (1998).
- [15] V. A. Godyak, R. B. Piejak, B. M. Alexandrovich, and V. I. Kolobov, *Phys. Rev. Lett.* **80**, 3264 (1998).
- [16] S. Takechi and S. Shinohara, *Jpn. J. Appl. Phys.* **38**, L148 (1999).
- [17] Yu. M. Aliev, I. D. Kaganovich, and H. Schlüter, *Phys. Plasmas* **4**, 2413 (1997).
- [18] V. A. Godyak, R. B. Piejak, and B. M. Alexandrovich, *Phys. Rev. Lett.* **83**, 1610 (1999).
- [19] R. B. Piejak and V. A. Godyak, *Appl. Phys. Lett.* **76**, 2188 (2000).
- [20] A. Smolyakov, V. Godyak, and A. Duffy, *Phys. Plasmas* **7**, 4755 (2000).
- [21] V. Godyak, B. Alexandrovich, R. Piejak, and A. Smolyakov, *Plasma Sources Sci. Technol.* **9**, 541 (2000).
- [22] R. H. Cohen and T. D. Rognlien, *Phys. Plasmas* **3**, 1839 (1966).
- [23] R. H. Cohen and T. D. Rognlien, *Plasma Sources Sci. Technol.* **5**, 442 (1996).
- [24] A. I. Smolyakov and I. Khabibrakhmanov, *Phys. Rev. Lett.* **81**, 4871 (1998).
- [25] C. Chung, S.-H. Seo, and H.-Y. Chang, *Phys. Plasmas* **7**, 3584 (2000).
- [26] J. D. Evans, F. F. Chen, and D. Arnush, in *Proceedings of the International Conference on Plasma Physics* (INRS Hydro-Quebec, Quebec, Canada, 2000), p. 916.
- [27] F. F. Chen, *Phys. Plasmas* (to be published).